

Rydberg spectrum of a single trapped Ca^+ ion: A Floquet analysis

Mariusz Pawlak^{1,2,*} and H. R. Sadeghpour²

¹*Faculty of Chemistry, Nicolaus Copernicus University in Toruń, Gagarina 7, 87-100 Toruń, Poland*

²*ITAMP, Harvard-Smithsonian Center for Astrophysics, Cambridge, Massachusetts 02138, USA*

We compute the Rydberg spectrum of a single Ca^+ ion in a Paul trap by incorporating various internal and external coupling terms of the ion to the trap in the Hamiltonian. The coupling terms include spin-orbit coupling in Ca^+ , charge (electron and ionic core) coupling to the radio frequency and static fields, ion-electron coupling in the Paul trap, and ion center-of-mass coupling. The electronic Rydberg states are precisely described by a one-electron model potential for $e^- + \text{Ca}^{2+}$, and accurate eigenenergies, quantum defect parameters, and static and tensor polarizabilities for a number of excited Rydberg states are obtained. The time-periodic rf Hamiltonian is expanded in the Floquet basis, and the trapping-field-broadened Rydberg lines are compared with recent observations of $\text{Ca}^+(23P)$ and $\text{Ca}^+(52F)$ Rydberg lines.

I. INTRODUCTION

Trapped Rydberg ions have recently come to the fore as promising candidates for fast quantum gate operations and long coherence times. The controllability and long coherence times of trapped ions, when augmented with precision and tunability of Rydberg excitations, offer tantalizing opportunities to leverage the best of the two schemes [1–4]. The realization of such quantum gates with long-range Rydberg and Coulomb interactions may be used in Rydberg ion crystals for entanglement operations in quantum information processing and computing applications [3, 5]. Additionally, trapped Rydberg ions possess enormous polarizabilities which can be manipulated with external fields [6], making them exquisite probes of their environments.

Trapped ions whose motional state fidelity is prone to decoherence due to fluctuating surface electric-field dipole noise [7–10] can be used to detect and probe residual electric fields present in Paul traps [4, 11, 12]. Rydberg atoms likewise have been shown to be sensitive probes of certain surfaces due to the presence of low electric fields [13].

The presence of static, dynamic, and stray fields in a Paul trap strongly modifies the Rydberg spectral properties of the ion. It was investigated theoretically in Refs. [5, 14], followed by the first realization of Rydberg F [4] and P [6] states in trapped Ca^+ ion, and the coherent control of a single trapped Rydberg Sr^+ ion in S states [2]. Accurate values for eigenenergies, transition rates, and multipole polarizabilities of low-excited states of Ca^+ in the absence of trapping fields were presented in Ref. [15].

In this work, we demonstrate details of a variational calculation of Paul-trap-induced $\text{Ca}^+(52F, 23P)$ Rydberg spectra. A parametric one-electron valence potential with spin-orbit coupling is used to describe the electronic structure of bare Ca^+ ions. The energy levels, transition dipole moments, and quantum defects for highly excited

ions are calculated for S , P , D , F , and G states (up to $n = 64$). The scalar and tensor polarizabilities for the Rydberg states are determined and compared with available values. A Floquet expansion is used to calculate the matrix elements with the coupling of the ion motion to the rf and electrodes' trap potentials. The resulting Rydberg spectra with additional peaks due to the field couplings are examined and compared with recent experimental findings [4]. Unless indicated otherwise, atomic units (a.u.) are used throughout.

II. THEORY AND COMPUTATION

A. Hamiltonian terms

The Hamiltonian of an atomic ion in a Paul trap can be written as [14]

$$\hat{H} = \hat{H}_e + \hat{H}_{\text{Ie}} + \hat{H}_{\text{I}}, \quad (1)$$

where \hat{H}_e is the electronic Hamiltonian for an ion in a Paul trap, \hat{H}_{Ie} is the Hamiltonian describing the atomic electron coupling to the trapped ion motion, and \hat{H}_{I} is the Hamiltonian for the motion of the ion in the trap. Each term is described in detail below.

1. Electron motion in the trap fields

The coupling of the valence electron to the trapping potentials (in a.u.) is given as

$$\hat{H}_e = \hat{H}_{\text{FF}} - \Phi(\mathbf{r}, t) + E_{\text{geom}z} \cos(\Omega_{\text{rf}} t), \quad (2)$$

where the first term on the right-hand side is the field-free Hamiltonian, describing a single free Ca^+ ion. The second term is the coupling of the electron to the linear Paul trap, and the last term is the residual electric field, which the ion is exposed to due to fabrication imperfections. The magnitude of this residual field is obtained from the broadening of the $4S-4P$ transition in Ca^+ [4]. Ω_{rf} is the rf frequency.

* teomar@chem.umk.pl

The field-free Hamiltonian is

$$\hat{H}_{\text{FF}} = -\frac{1}{2}\Delta_{\mathbf{r}} + V_l(r) + V_{\text{LS}}(r), \quad (3)$$

where the valence electron interacts with all other electrons via an effective nonlocal parametric potential [16]:

$$V_l(r) = -\frac{1}{r} \left(2 + (Z-2)e^{-a_1^{(l)}r} + a_2^{(l)}r e^{-a_3^{(l)}r} \right) - \frac{\alpha_c}{2r^4} \left(1 - e^{-(r/r_c^{(l)})^6} \right), \quad (4)$$

with Z being the ion nuclear charge. The last term in Eq. (4) is the core polarization potential, wherein α_c is the electric dipole polarizability of the doubly charged ionic core and $r_c^{(l)}$ is a cutoff radius which ensures the proper behavior of the potential near the origin. The l -dependent parameters ($a_1^{(l)}$, $a_2^{(l)}$, $a_3^{(l)}$, and $r_c^{(l)}$) fitted to experimental energy levels are available for different alkaline-earth-metal ions in Ref. [16].

The spin-orbit coupling is

$$V_{\text{LS}}(r) = \frac{\alpha_{\text{LS}}^2}{2} \frac{1}{r} \frac{dV_l(r)}{dr} \left(1 - \frac{\alpha_{\text{LS}}^2}{2} V_l(r) \right)^{-2} \hat{\mathbf{L}} \cdot \hat{\mathbf{S}}, \quad (5)$$

where α_{LS} is the fine-structure constant, and $\langle \hat{\mathbf{L}} \cdot \hat{\mathbf{S}} \rangle = [j(j+1) - l(l+1) - 3/4]/2$. The total electronic angular momentum quantum $j = l \pm \frac{1}{2}$.

The coupling of the electron to the linear Paul trap includes two terms,

$$-\Phi(\mathbf{r}, t) = \hat{H}_{\text{trap}}^{\text{rf}} + \hat{H}_{\text{trap}}^{\text{dc}} = -\alpha \cos(\Omega_{\text{rf}}t)(x^2 - y^2) + \beta(x^2 + y^2 - 2z^2), \quad (6)$$

where α and β are the rf and static electric field gradients, respectively, and (x, y, z) are the electron coordinates.

Finally, the trap imperfection alternating residual electric field amplitude, see the third term in Eq. (2), is written explicitly as [4]

$$E_{\text{geom}} = 0.8(U_{\text{rf}}/m) \sin(\Omega_{\text{rf}}t), \quad (7)$$

where U_{rf} is the rf voltage. The numerical coefficient in Eq. (7) may be different for different ion traps.

2. Electron motion coupled to trapped ion motion

In a highly excited Rydberg state, the spatial extent of the electron wave function can become larger than the oscillator length, and the coupling of the electronic and external motional degrees of freedom needs to be accounted for. The Hamiltonian for the Rydberg electron coupling to the ion motion (in a.u.) is

$$\hat{H}_{\text{Ie}} = \hat{H}_{\text{Ie}}^{\text{rf}} + \hat{H}_{\text{Ie}}^{\text{dc}} = -2\alpha \cos(\Omega_{\text{rf}}t)(xX - yY) + 2\beta(xX + yY - 2zZ), \quad (8)$$

where (X, Y, Z) are the ion coordinates in the trap.

3. Ion motion in the trap

The Hamiltonian for the ion center-of-mass motion in the trap is expressed as (in a.u.)

$$\hat{H}_{\text{I}} = -\frac{1}{2M}\Delta_{\mathbf{R}} + \Phi(\mathbf{R}, t). \quad (9)$$

The static field and the rapidly oscillating rf field form an effective time-independent harmonic potential [14, 17],

$$\Phi(\mathbf{R}, t) \simeq \frac{M}{2} \sum_{\rho=X,Y,Z} \omega_{\rho}^2 \rho^2, \quad (10)$$

where M is the mass of the ion and

$$\omega_X = \omega_Y = \sqrt{2[(\alpha/(M\Omega_{\text{rf}}))^2 - \beta/M]}, \quad (11)$$

$$\omega_Z = 2\sqrt{\beta/M},$$

are respectively, the transverse and axial trap frequencies.

The total Hamiltonian in Eq. (1), when grouped for computational efficiency, is

$$\hat{H} = \hat{H}_{\text{FF}} + [\hat{H}_{\text{trap}}^{\text{rf}} + \hat{H}_{\text{trap}}^{\text{dc}}] + \hat{H}_{\text{geom}} + [\hat{H}_{\text{Ie}}^{\text{rf}} + \hat{H}_{\text{Ie}}^{\text{dc}}] + \hat{H}_{\text{I}}. \quad (12)$$

B. Solutions to the field-free Hamiltonian

We are interested in the bound eigenstate spectrum of the stationary time-independent Schrödinger equation describing the valence electron motion in Ca^+ :

$$\hat{H}_{\text{FF}}\Psi = E\Psi. \quad (13)$$

The bound states of this Hamiltonian are expanded in the L^2 basis, $\varphi_k(r)Y_{l,m}(\theta, \phi)$, where $\varphi_k = r^{\zeta-1}e^{-\gamma_k r}$ are Slater-type orbitals (STOs), with ζ and γ_k as the optimization parameters. Because STOs are not orthogonal, we diagonalize the overlap matrix \mathbf{S} : $\boldsymbol{\lambda} = \mathbf{V}^T \mathbf{S} \mathbf{V}$, where $\boldsymbol{\lambda}$ is a diagonal matrix of positive eigenvalues and \mathbf{V} is an orthogonal eigenvector matrix. Next, we transform the radial part of the basis set to an orthonormal form:

$$\tilde{\varphi}_p(r) = \frac{1}{\sqrt{\lambda_{p,p}}} \sum_k V_{k,p} \varphi_k(r). \quad (14)$$

Matrix elements of the field-free Hamiltonian in the orthonormal basis set are

$$[\mathbf{H}_{\text{FF}}]_{i',i} = \frac{\delta_{l',l} \delta_{m',m}}{\sqrt{\lambda_{p',p'} \lambda_{p,p}}} \sum_{k',k} V_{k',p'}^* \langle \varphi_{k'} | \hat{H}_{\text{FF}} | \varphi_k \rangle V_{k,p}. \quad (15)$$

This variational approach allows us to calculate accurately the field-free energy spectrum for any arbitrary (l, j) sets. The trial space is spanned by 660 STOs. The optimization procedure and the details for calculating the matrix elements of the Hamiltonian are provided in

Ref. [18]. The energies resulting from the diagonalization of \mathbf{H}_{FF} are fully converged with respect to basis set size. The energies and wave functions also behave properly with respect to the spin-orbit splitting, which decreases with increasing orbital quantum number.

The radial field-free eigenfunctions are

$$\psi_n(r) = \sum_p \frac{C_{p,n}^{(l,j)}}{\sqrt{\lambda_{p,p}}} \sum_k V_{k,p} \varphi_k(r), \quad (16)$$

where the expansion coefficients $C_{p,n}^{(l,j)}$ are from the eigenvector matrix of \mathbf{H}_{FF} .

The eigenenergies are used to determine the quantum defects $\delta_{l,j}$. Within the quantum defect theory approach, the energy levels of the system with one valence electron are given by [19, 20]

$$E_{n,l,j} = -\frac{Z_c^2}{2(n - \delta_{l,j}(n))^2}, \quad (17)$$

where Z_c is the ionic core charge and n is the principal quantum number. For highly excited states, it is often sufficient to take $\delta_{l,j}(n)$ as a constant. For lower excitations, the Ritz expansion is applied:

$$\delta_{l,j}(n) = \delta_0^{l,j} + \frac{\delta_2^{l,j}}{(n - \delta_0^{l,j})^2} + \frac{\delta_4^{l,j}}{(n - \delta_0^{l,j})^4} + \dots \quad (18)$$

The scalar (α_0) and tensor (α_2) polarizabilities of the $\text{Ca}^+(52l)$ Rydberg states are calculated as [21, 22]

$$\alpha_0 = -\frac{2}{3} \sum_{n',l',j'} (2j' + 1) l_{>} \left\{ \begin{matrix} l & j & \frac{1}{2} \\ j' & l' & 1 \end{matrix} \right\}^2 \frac{|\langle nl|r|n'l' \rangle|^2}{E_{n,l,j} - E_{n',l',j'}}, \quad (19)$$

$$\alpha_2 = -2 \sqrt{\frac{10j(2j-1)(2j+1)}{3(j+1)(2j+3)}} \sum_{n',l',j'} (-1)^{j+j'} (2j' + 1) l_{>} \times \left\{ \begin{matrix} l & j & \frac{1}{2} \\ j' & l' & 1 \end{matrix} \right\}^2 \left\{ \begin{matrix} j & j' & 1 \\ 1 & 2 & j \end{matrix} \right\} \frac{|\langle nl|r|n'l' \rangle|^2}{E_{n,l,j} - E_{n',l',j'}}, \quad (20)$$

where $l_{>}$ is the greater of l and l' . The total polarizability of a state with non-zero total angular momentum is [23]

$$\alpha_{\text{tot}} = \alpha_0 + \alpha_2 \frac{3m_j^2 - j(j+1)}{j(2j-1)}, \quad (21)$$

with $-j \leq m_j \leq j$.

C. Floquet solutions to the time-periodic Hamiltonian

Since the Hamiltonian is time periodic, we expand the solutions in a Floquet basis [24–28], leading to the eigen-

value equation (in a.u.)

$$\hat{\mathcal{H}}_{\mathcal{F}} \mathcal{Y}_{\varepsilon}(\mathbf{R}, \mathbf{r}, t) = \left(\hat{H} - i \frac{\partial}{\partial t} \right) \mathcal{Y}_{\varepsilon}(\mathbf{R}, \mathbf{r}, t) = \varepsilon \mathcal{Y}_{\varepsilon}(\mathbf{R}, \mathbf{r}, t), \quad (22)$$

where $\hat{\mathcal{H}}_{\mathcal{F}}$ is the Floquet Hamiltonian and $\mathcal{Y}_{\varepsilon}(\mathbf{r}, \mathbf{R}, t)$ are time-periodic wave functions with period $2\pi/\Omega_{\text{rf}}$,

$$\mathcal{Y}_{\varepsilon}(\mathbf{r}, \mathbf{R}, t) = \mathcal{Y}_{\varepsilon} \left(\mathbf{r}, \mathbf{R}, t + \frac{2\pi}{\Omega_{\text{rf}}} \right) = \sum_{q=-\infty}^{\infty} e^{iq\Omega_{\text{rf}}t} \Xi_{\varepsilon}^q(\mathbf{r}, \mathbf{R}). \quad (23)$$

The time-independent components $\Xi_{\varepsilon}^q(\mathbf{r}, \mathbf{R})$ are usually called the Floquet channel functions. They fulfill the relationship

$$\Xi_{\varepsilon}^q(\mathbf{r}, \mathbf{R}) = \Xi_{\varepsilon+g\Omega_{\text{rf}}}^{q+g}(\mathbf{r}, \mathbf{R}) \quad (24)$$

for any integer g . We represent each component in the basis set

$$\xi_{\eta}(\mathbf{r}, \mathbf{R}) = \psi_n(r) Y_{l,m}(\theta, \phi) \prod_{\rho=X,Y,Z} \psi_{k_{\rho}}(\rho), \quad (25)$$

where η is a superindex containing the quantum numbers $\{n, l, m, k_X, k_Y, k_Z\}$. Solutions of a three-dimensional quantum harmonic oscillator, $\prod_{\rho=X,Y,Z} \psi_{k_{\rho}}(\rho)$, are used here as a part of the basis set, since by Eq. (10)

$$\left\langle \prod_{\rho=X,Y,Z} \psi_{k'_{\rho}} \left| \hat{H}_1 \right| \prod_{\rho=X,Y,Z} \psi_{k_{\rho}} \right\rangle = \sum_{\rho=X,Y,Z} \omega_{\rho} \left(k_{\rho} + \frac{1}{2} \right) \delta_{k'_{\rho} k_{\rho}}, \quad (26)$$

where k_{ρ} are the harmonic oscillator quantum numbers.

Then, the Floquet–Hamiltonian matrix is expressed as

$$[\mathcal{H}_{\mathcal{F}}]_{q',\eta',q,\eta} = \frac{\Omega_{\text{rf}}}{2\pi} \int_0^{2\pi/\Omega_{\text{rf}}} \langle \xi_{\eta'}(\mathbf{r}, \mathbf{R}) | \hat{H}(\mathbf{r}, \mathbf{R}, t) | \xi_{\eta}(\mathbf{r}, \mathbf{R}) \rangle \times e^{i(q-q')\Omega_{\text{rf}}t} dt + q\Omega_{\text{rf}} \delta_{q',q} \delta_{\eta',\eta}. \quad (27)$$

Since the rf field in the Paul trap is sinusoidal, the Floquet–Hamiltonian matrix is reduced to the following form:

$$[\mathcal{H}_{\mathcal{F}}]_{q',q} = [\mathbf{E} + \mathbf{H}_{\text{trap}}^{\text{dc}} + \mathbf{H}_{\text{Ie}}^{\text{dc}} + \mathbf{H}_{\text{I}} + q\Omega_{\text{rf}}\mathbf{I}] \delta_{q',q} + \frac{1}{2} [\mathbf{H}_{\text{trap}}^{\text{rf}} + \mathbf{H}_{\text{Ie}}^{\text{rf}} + \mathbf{H}_{\text{geom}}] \delta_{q',q\pm 1}. \quad (28)$$

The explicit expressions for the matrix elements are given in the Appendix. Analytical solutions for all the angular matrix elements are reported in the Supporting Information of Ref. [29]. To construct the supermatrix in Eq. (28), the $\text{Ca}^+(n \leq 64, l \leq 4, |m| \leq l, j = l - 1/2)$ 12 photon absorption and emission transitions are considered ($q = -12, -11, \dots, 11, 12$). Since the calculations are time-consuming, the ion is assumed to be in the ground motional state ($k_X = k_Y = k_Z = 0$). This approximation is physically motivated, since the mass of the ionic core is much larger than the mass of the valence electron.

Equation (28) can be, in general, presented in matrix form as

TABLE I. The low-lying $nD_{3/2}$ and high-lying $nF_{5/2}$ and $nP_{1/2}$ energy levels of Ca^+ . The presented results are compared with Ref. [31], where the spin-orbit splitting is neglected, and with Ref. [6]. The calculated transition dipole moments, $d_{DF} = \langle 3D_{3/2} | r | nF_{5/2} \rangle$ and $d_{DP} = \langle 3D_{3/2} | r | nP_{1/2} \rangle$, are given in the last column. The values are in atomic units.

$E_{nD} (\times 10^{-1})$		$E_{nD_{3/2}} (\times 10^{-1})$	
n	Ref. [31]	This work	
3	-3.73917	-3.74136	
4	-1.77235	-1.77338	
5	-1.04894	-1.04878	
6	-0.693570	-0.693448	
7	-0.492592	-0.492543	
8	-0.367889	-0.367876	
9	-0.285204	-0.285207	
10	-0.227570	-0.227579	

n	$E_{nF} (\times 10^{-3})$ Ref. [31]	$E_{nF_{5/2}} (\times 10^{-3})$ Ref. [6]	$E_{nF_{5/2}} (\times 10^{-3})$ This work	$d_{DF} (\times 10^{-2})$ This work
45	-0.988791	-0.988929	-0.988967	2.38399
46	-0.946244	-0.946373	-0.946408	2.30637
47	-0.906385	-0.906505	-0.906539	2.23288
48	-0.868992	-0.869106	-0.869137	2.16321
49	-0.833867	-0.833973	-0.834003	2.09709
50	-0.800829	-0.800929	-0.800957	2.03428
51	-0.769716	-0.769810	-0.769837	1.97457
52	-0.740382	-0.740471	-0.740496	1.91769
53	-0.712693	-0.712777	-0.712801	1.86350
54	-0.686529	-0.686609	-0.686631	1.81182
55	-0.661780	-0.661855	-0.661876	1.76249

n	$E_{nP} (\times 10^{-2})$ Ref. [31]	$E_{nP_{1/2}} (\times 10^{-2})$ Ref. [6]	$E_{nP_{1/2}} (\times 10^{-2})$ This work	$d_{DP} (\times 10^{-3})$ This work
20	-0.580433	-0.580421	-0.580590	8.07380
21	-0.522603	-0.522596	-0.522737	7.45575
22	-0.473006	-0.473002	-0.473120	6.91301
23	-0.430148	-0.430147	-0.430247	6.43329
24	-0.392862	-0.392862	-0.392948	6.00677
25	-0.360222	-0.360223	-0.360298	5.62551
26	-0.331487	-0.331489	-0.331554	5.28306
27	-0.306059	-0.306061	-0.306118	4.97408
28	-0.283448	-0.283450	-0.283500	4.69415
29	-0.263253	-0.263256	-0.263300	4.43958
30	-0.245142	-0.245145	-0.245184	4.20727

0.02902(2) [6]. The goodness of our fit, within a non-linear least-squares procedure, is as follows: the sum of squares due to error, also known as the sum of squares of residuals, is less than 2.2×10^{-9} , the root-mean-squared error is less than 6.1×10^{-6} , whereas the coefficient of determination (R^2) for the worst case is equal to one with an accuracy to seven decimal places.

A good measure of the accuracy of our wave functions and energies are the static and tensor polarizabilities for Rydberg states, as the polarizability is an acutely sensitive parameter of the linear response the-

TABLE II. Calculated quantum defect parameters in Eq. (18) for Ca^+ in different S , P , D , F , and G states.

Level	$\delta_0^{l,j}$	$\delta_2^{l,j}$	$\delta_4^{l,j}$
$nS_{1/2}$	1.80149622	0.201535974	0.312279201
$nP_{1/2}$	1.43927290	0.331987211	0.687628538
$nP_{3/2}$	1.43532329	0.332803651	0.690740476
$nD_{3/2}$	0.627759022	-0.0148289072	1.98904443
$nD_{5/2}$	0.627066817	-0.0128801411	1.96257423
$nF_{5/2}$	0.0298974503	-0.202650265	0.497416258
$nF_{7/2}$	0.0296853803	-0.198110426	0.457337917
$nG_{7/2}$	0.00614904531	-0.0419102731	0.0164937590
$nG_{9/2}$	0.00614352002	-0.0418535034	0.0717188390

TABLE III. The scalar, α_0 , and tensor, α_2 , polarizabilities of the Rydberg states of Ca^+ . All the values are in $\text{MHz}/(\text{V}/\text{cm})^2$.

Level	α_0		α_2	
	This work	Ref. [23]	This work	Ref. [23]
$52P$		-69.774		15.137
$52P_{1/2}$	-69.836		0.000	
$52P_{3/2}$	-68.519		14.980	
$52D$		32.149		-39.221
$52D_{3/2}$	31.857		-27.559	
$52D_{5/2}$	31.260		-38.421	
$52F$		—		—
$52F_{5/2}$	582.449		-212.689	
$52F_{7/2}$	587.395		-250.175	

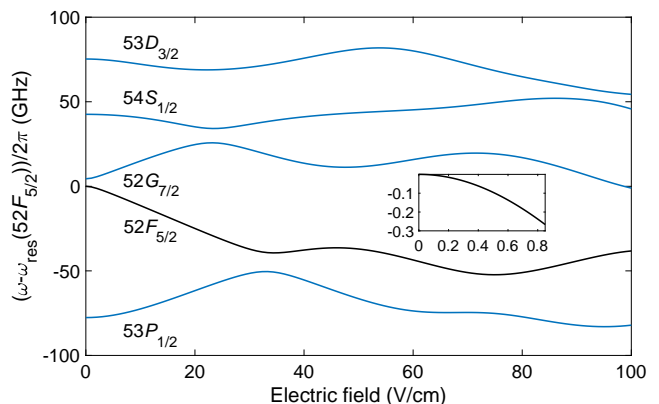


FIG. 1. Stark map of Ca^+ near the $52F$ level showing the mixing of Rydberg states with different angular momenta in an electric field. As the inset indicates, at small fields, relevant to experimental values, the $52F$ -state energy shift is quadratic in the field and there is no field mixing.

ory to perturbations by external fields. The static scalar and tensor polarizabilities are defined in Eqs. (19) and (20). We calculate the $\text{Ca}^+(n = 52)$ Rydberg polarizabilities, presented in Table III, and compared with available values from literature [23]. The summation in

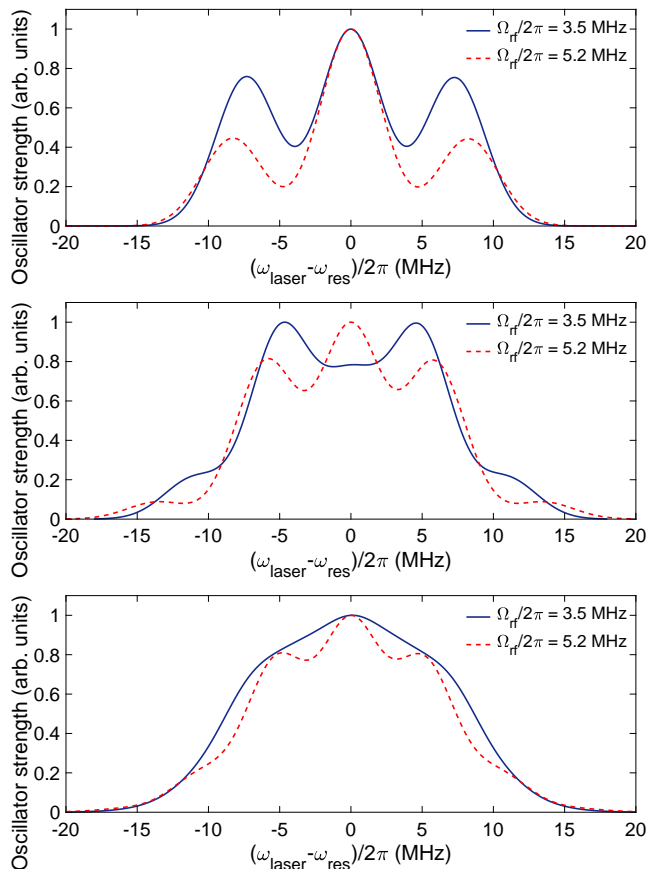


FIG. 2. The Mollow triplet effect around the zero detuning of $3D_{3/2}$ to $52F_{5/2}$ transition line, when $\Omega_{\text{rf}}/2\pi = 3.5$ (solid curve) and 5.2 (dashed curve) MHz. The rf and static field gradients are $\alpha = 8.52 \times 10^6$ V/m² and $\beta = 3.32 \times 10^4$ V/m², respectively. The residual electric field is not considered in these calculations, i.e., $E_{\text{geom}} = 0$. Upper panel: The calculations limited to 1-photon processes, by including 3 Floquet channels, i.e., $(-1, 0, +1)$. Middle panel: The calculations limited to 2-photon processes (5 Floquet channels). Lower panel: Up to 12-photon processes allowed (25 Floquet channels). The Gaussian convolution is performed on the calculated results by considering a 5-MHz laser linewidth.

Eqs. (19) and (20) is performed over bound states up to $n' = 64$. The experimentally determined $\alpha_{\text{tot}}(52F) = 10_{-3}^{+7} \times 10^2$ MHz/(V/cm)² [4, 33] is in agreement with the theoretical results in Table III, i.e., $\alpha_{\text{tot}}(52F_{5/2}) = 752.600$ and $\alpha_{\text{tot}}(52F_{7/2}) = 766.091$ MHz/(V/cm)².

Polarizability is proportional to the squares of transition dipole moments and inversely proportional to the energy differences [see Eqs. (19) and (20)], and thus the polarizability of the nF states is significantly larger in comparison with the polarizability for the separated states with not-negligible quantum defects ($l < 3$ states in Table II) [34]. The main contribution to the polarizability of the $52F$ state comes from the coupling to the nearby $52G$ state. Figure 1 shows the Stark map of Ca^+ eigenstates in the vicinity of the $52F$ state up to 100 V/cm. Electric fields in the ion traps are usually less than 1 V/cm [35];

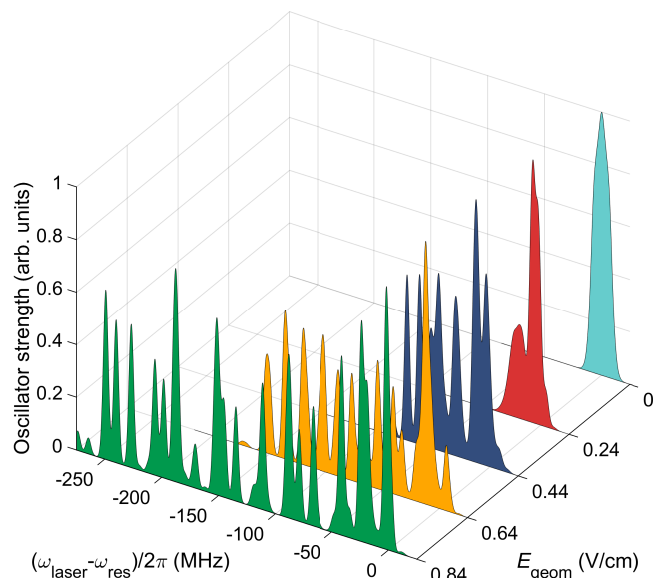


FIG. 3. The normalized oscillator strength for the $\text{Ca}^+(3D_{3/2} \rightarrow 52F_{5/2})$ resonant transition at various E_{geom} . Correspondingly, $\alpha = 8.52 \times 10^6$ V/m², $\beta = 3.32 \times 10^4$ V/m², and $\Omega_{\text{rf}}/2\pi = 3.5$ MHz. Up to ± 12 photons in absorption and emission are included in the Floquet calculations for convergence. The Gaussian convolution is performed on the calculated results by considering a 5-MHz laser linewidth.

at such low electric fields, the F state is well isolated from the G state. As expected, the inset of Fig. 1 shows that for small fields the energy shift remains quadratic and there is no field mixing.

B. Trap-induced Rydberg spectra

We investigate the spectroscopic features of the $\text{Ca}^+(3D_{3/2}) + h\nu \rightarrow \text{Ca}^+(nF_{5/2})$ transition line when a single Ca^+ ion is confined in a Paul trap. We start with $E_{\text{geom}} = 0$ in Eq. (2). The coupling of the electron to the linear Paul trap, Eq. (6), is considered with the rf ($\alpha = 8.52 \times 10^6$ V/m²) and the electrode ($\beta = 3.32 \times 10^4$ V/m²) field gradients. Multiphoton absorption and emission Floquet transitions, i.e., $\text{Ca}^+(3D_{3/2}) + qh\nu \rightarrow \text{Ca}^+(nF_{5/2})$, with up to $q = 12$ photons absorbed and emitted, are considered.

Figure 2 shows the Mollow triplets formed near the $\text{Ca}^+(52F)$ Rydberg line, for two experimental rf frequencies, $\Omega_{\text{rf}}/2\pi = 3.5$ and 5.2 MHz [4] with different Floquet channels (1-photon, 2-photon, and 12-photon absorption and emission). In the lower panel of Fig. 2, the separation between the two outer peaks is $2\Omega_{\text{rf}}$, indicating the convergence of the results. Note that the calculated oscillator strengths are convoluted with a Gaussian laser linewidth of 5 MHz full width at half maximum. As this linewidth is greater than the rf frequency, $\Omega_{\text{rf}}/2\pi = 3.5$ MHz (solid blue curve), only one broad

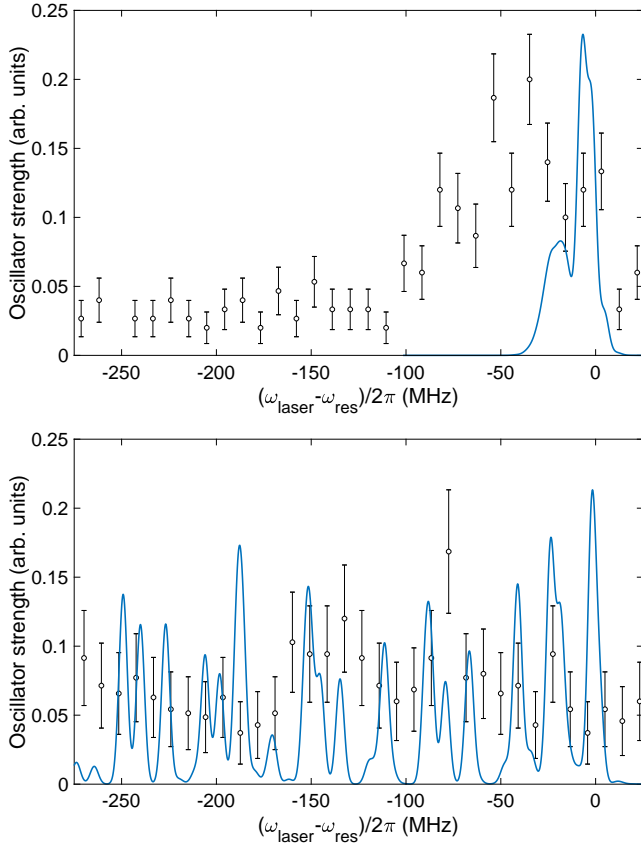


FIG. 4. The oscillator strength for the $\text{Ca}^+(3D_{3/2} \rightarrow 52F_{5/2})$ resonant transition with $E_{\text{geom}} = 0.24$ V/cm (upper panel), and $E_{\text{geom}} = 0.84$ V/cm (lower panel). The transverse and longitudinal trap frequencies are $\omega_{\text{radial}}/2\pi = 200$ kHz and $\omega_{\text{axial}}/2\pi = 90$ kHz, respectively. The parameters used are the same as those in Fig. 3. Experimental data are courtesy of the Mainz group [36] and the error bars depict the quantum projection noise. The Gaussian convolution is performed on the calculated results by considering a 5-MHz laser linewidth.

maximum is visible. The coupling in the Mollow triplet is due to the electron-trap interaction, Eq. (6). The $\hat{H}_{\text{trap}}^{\text{rf}}$ matrix elements obey the $\Delta l = 0, 2$ and $\Delta m = \pm 2$ selection rules, while the $\hat{H}_{\text{trap}}^{\text{dc}}$ matrix elements select the $\Delta l = 0, 2$ and $\Delta m = 0$ transitions.

The effect of the residual electric field, E_{geom} , on the spectral line, $3D_{3/2} \rightarrow 52F_{5/2}$, is examined in Fig. 3. The calculated oscillator strengths for this transition are shown for different values of the residual electric field, $0 \leq E_{\text{geom}} \leq 0.84$ V/cm. The transition matrix elements are integrated over the ground motional state of the trap, e.g., Eq. (26). Spectral convolution is carried out by a Gaussian function with the 5-MHz laser linewidth. In Fig. 4, the calculated oscillator strengths are compared with the observed spectra [4, 33], at $E_{\text{geom}} = 0.24$ and 0.84 V/cm. As observed in the experiment, the calculated line shape of the resonance confirms the strong state-dependent coupling to the static and oscillatory electric field potentials in the trap.

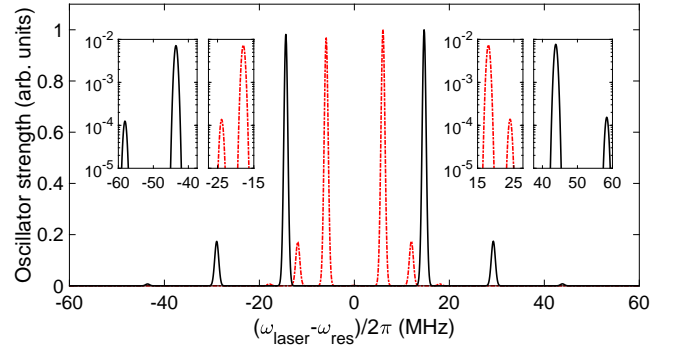


FIG. 5. The normalized oscillator strength for the $\text{Ca}^+(3D_{3/2} \rightarrow 23P_{1/2})$ resonance transition with $E_{\text{geom}} = 1.6$ V/cm, $\Omega_{\text{rf}}/2\pi = 14.56$ MHz, $\alpha = 3.161 \times 10^8$ V/m², and $\beta = 1.286 \times 10^6$ V/m² (solid black line) and $E_{\text{geom}} = 0.1$ V/cm, $\Omega_{\text{rf}}/2\pi = 5.98$ MHz, $\alpha = 1.298 \times 10^8$ V/m², and $\beta = 1.286 \times 10^6$ V/m² (dashed-dotted red line). These results in black and red should be compared with the experimental spectra in Figs. 2(b) and 2(c) in Ref. [6], respectively. In particular, the formation of Rydberg side bands at about ± 45 and ± 55 MHz are visible in the inset plots and detected in the experiment. A 1-MHz laser linewidth is used for the Gaussian convolution of the calculated spectra.

Figure 5 presents the calculated oscillator strength for the $\text{Ca}^+(3D_{3/2} \rightarrow 23P_{1/2})$ transition for two sets of trap parameters, as in Ref. [6]: $E_{\text{geom}} = 1.6$ V/cm, $\Omega_{\text{rf}}/2\pi = 14.56$ MHz, $\alpha = 3.161 \times 10^8$ V/m², and $\beta = 1.286 \times 10^6$ V/m²; and $E_{\text{geom}} = 0.1$ V/cm, $\Omega_{\text{rf}}/2\pi = 5.98$ MHz, $\alpha = 1.298 \times 10^8$ V/m², and $\beta = 1.286 \times 10^6$ V/m². The results are convoluted with a Gaussian function of 1-MHz laser linewidth. The peaks, including small far-detuned bumps, agree almost perfectly with the maxima in the experimental spectra in Figs. 2(b) and 2(c) in Ref. [6].

IV. SUMMARY AND OUTLOOK

This work is a description of the first fully variational calculation of the Rydberg spectra of a single ion in a Paul trap. All relevant coupling terms in the Hamiltonian of the ion in the trap are accounted for. The time-periodic rf field is treated nonperturbatively within the Floquet formalism. The motional state of the ion in the trap is also considered. The quantum defect parameters and static and tensor dipole polarizabilities for highly excited states of Ca^+ are obtained and compared with available measurements. Precise trapped-induced Rydberg ion [$\text{Ca}^+(52F)$ and $\text{Ca}^+(23P)$] spectra are calculated. These spectra with their sensitivity to trap or external static and time-varying fields can be used as exquisite probes of residual and stray electric field fluctuations near electrode surfaces and for quantum nonequilibrium dynamics of ion qubits. The extremely large polarizabilities of and controlled long-range interactions between Rydberg states can be employed for ion imaging [37]. Future studies of qubit operation, fidelity, and

fast computation with trapped Rydberg ions should benefit from such spectral analysis.

ACKNOWLEDGMENTS

We are grateful to the Mainz group (Schmidt-Kaler and Mokhberi) for extremely valuable discussions and access to the experimental data used here. M.P. thanks the National Science Centre, Poland, for financial sup-

port under Grant No. 2017/01/X/ST4/00326. H.R.S. acknowledges the support from the NSF through a grant for ITAMP at Harvard University.

APPENDIX

Matrix elements of the terms of the time-independent Floquet–Hamiltonian, presented in Eq. (28), with the basis set $\{\xi_\eta\}$, Eq. (25), are explicitly given below:

$$[\mathbf{E}]_{\eta',\eta} = E_{n,l,j} \delta_{n',n} \delta_{l',l} \delta_{m',m} \delta_{k'_X,k_X} \delta_{k'_Y,k_Y} \delta_{k'_Z,k_Z}, \quad (\text{A.1})$$

$$\begin{aligned} [\mathbf{H}_{\text{trap}}^{\text{dc}}]_{\eta',\eta} &= \beta \langle \xi_{\eta'} | x^2 + y^2 - 2z^2 | \xi_\eta \rangle \\ &= \beta \langle \psi_{n'} | r^2 | \psi_n \rangle (\delta_{l',l} \delta_{m',m} - 3 \langle Y_{l',m'} | \cos^2 \theta | Y_{l,m} \rangle) \delta_{k'_X,k_X} \delta_{k'_Y,k_Y} \delta_{k'_Z,k_Z}, \end{aligned} \quad (\text{A.2})$$

$$\begin{aligned} [\mathbf{H}_{\text{Ie}}^{\text{dc}}]_{\eta',\eta} &= 2\beta \langle \xi_{\eta'} | xX + yY - 2zZ | \xi_\eta \rangle \\ &= 2\beta \langle \psi_{n'} | r | \psi_n \rangle (\langle Y_{l',m'} | \sin \theta \cos \phi | Y_{l,m} \rangle \langle \psi_{k'_X} | X | \psi_{k_X} \rangle \delta_{k'_Y,k_Y} \delta_{k'_Z,k_Z} \\ &\quad + \langle Y_{l',m'} | \sin \theta \sin \phi | Y_{l,m} \rangle \langle \psi_{k'_Y} | Y | \psi_{k_Y} \rangle \delta_{k'_X,k_X} \delta_{k'_Z,k_Z} \\ &\quad - 2 \langle Y_{l',m'} | \cos \theta | Y_{l,m} \rangle \langle \psi_{k'_Z} | Z | \psi_{k_Z} \rangle \delta_{k'_X,k_X} \delta_{k'_Y,k_Y}), \end{aligned} \quad (\text{A.3})$$

$$[\mathbf{H}_{\text{I}}]_{\eta',\eta} = \delta_{n',n} \delta_{l',l} \delta_{m',m} \sum_{\rho=X,Y,Z} \omega_\rho \left(k_\rho + \frac{1}{2} \right) \delta_{k'_\rho,k_\rho}, \quad (\text{A.4})$$

$$[\mathbf{I}]_{\eta',\eta} = \delta_{n',n} \delta_{l',l} \delta_{m',m} \delta_{k'_X,k_X} \delta_{k'_Y,k_Y} \delta_{k'_Z,k_Z}, \quad (\text{A.5})$$

$$\begin{aligned} [\mathbf{H}_{\text{trap}}^{\text{rf}}]_{\eta',\eta} &= -\alpha \langle \xi_{\eta'} | x^2 - y^2 | \xi_\eta \rangle \\ &= -\alpha \langle \psi_{n'} | r^2 | \psi_n \rangle (\langle Y_{l',m'} | \sin^2 \theta \cos^2 \phi | Y_{l,m} \rangle \\ &\quad - \langle Y_{l',m'} | \sin^2 \theta \sin^2 \phi | Y_{l,m} \rangle) \delta_{k'_X,k_X} \delta_{k'_Y,k_Y} \delta_{k'_Z,k_Z}, \end{aligned} \quad (\text{A.6})$$

$$\begin{aligned} [\mathbf{H}_{\text{Ie}}^{\text{rf}}]_{\eta',\eta} &= -2\alpha \langle \xi_{\eta'} | xX - yY | \xi_\eta \rangle \\ &= -2\alpha \langle \psi_{n'} | r | \psi_n \rangle (\langle Y_{l',m'} | \sin \theta \cos \phi | Y_{l,m} \rangle \langle \psi_{k'_X} | X | \psi_{k_X} \rangle \delta_{k'_Y,k_Y} \delta_{k'_Z,k_Z} \\ &\quad - \langle Y_{l',m'} | \sin \theta \sin \phi | Y_{l,m} \rangle \langle \psi_{k'_Y} | Y | \psi_{k_Y} \rangle \delta_{k'_X,k_X} \delta_{k'_Z,k_Z}), \end{aligned} \quad (\text{A.7})$$

$$\begin{aligned} [\mathbf{H}_{\text{geom}}]_{\eta',\eta} &= E_{\text{geom}} \langle \xi_{\eta'} | z | \xi_\eta \rangle \\ &= E_{\text{geom}} \langle \psi_{n'} | r | \psi_n \rangle \langle Y_{l',m'} | \cos \theta | Y_{l,m} \rangle \delta_{k'_X,k_X} \delta_{k'_Y,k_Y} \delta_{k'_Z,k_Z}, \end{aligned} \quad (\text{A.8})$$

where η denotes a superindex containing quantum numbers $\{n, l, m, k_X, k_Y, k_Z\}$. Simple expressions for the

above angular matrix elements are reported in the Supporting Information in Ref. [29].

[1] F. Engel, T. Dieterle, T. Schmid, C. Tomschitz, C. Veit, N. Zuber, R. Löw, T. Pfau, and F. Meinert, “Observation of Rydberg blockade induced by a single ion,”

Phys. Rev. Lett. **121**, 193401 (2018).

- [2] G. Higgins, F. Pokorny, C. Zhang, Q. Bodart, and M. Hennrich, “Coherent control of a single trapped Rydberg ion,” *Phys. Rev. Lett.* **119**, 220501 (2017).
- [3] G. Higgins, W. Li, F. Pokorny, C. Zhang, F. Kress, C. Maier, J. Haag, Q. Bodart, I. Lesanovsky, and M. Hennrich, “Single strontium Rydberg ion confined in a Paul trap,” *Phys. Rev. X* **7**, 021038 (2017).
- [4] T. Feldker, P. Bachor, M. Stappel, D. Kolbe, R. Gerritsma, J. Walz, and F. Schmidt-Kaler, “Rydberg excitation of a single trapped ion,” *Phys. Rev. Lett.* **115**, 173001 (2015).
- [5] M. Müller, L. Liang, I. Lesanovsky, and P. Zoller, “Trapped Rydberg ions: From spin chains to fast quantum gates,” *New J. Phys.* **10**, 093009 (2008).
- [6] A. Mokhberi, J. Vogel, J. Andrijauskas, P. Bachor, J. Walz, and F. Schmidt-Kaler, “Determination of quantum defect for the Rydberg P series of Ca II,” *J. Phys. B: At., Mol. Opt. Phys.* **52**, 214001 (2019).
- [7] D. A. Hite, Y. Colombe, A. C. Wilson, D. T. C. Allcock, D. Leibfried, D. J. Wineland, and D. P. Pappas, “Surface science for improved ion traps,” *MRS Bulletin* **38**, 826 (2013).
- [8] A. Safavi-Naini, P. Rabl, P. F. Weck, and H. R. Sadeghpour, “Microscopic model of electric-field-noise heating in ion traps,” *Phys. Rev. A* **84**, 023412 (2011).
- [9] A. Safavi-Naini, E. Kim, P. F. Weck, P. Rabl, and H. R. Sadeghpour, “Influence of monolayer contamination on electric-field-noise heating in ion traps,” *Phys. Rev. A* **87**, 023421 (2013).
- [10] K. Lakhmanskii, P. C. Holz, D. Schärfl, B. Ames, R. Assouly, T. Monz, Y. Colombe, and R. Blatt, “Observation of superconductivity and surface noise using a single trapped ion as a field probe,” *Phys. Rev. A* **99**, 023405 (2019).
- [11] D. A. Hite, Y. Colombe, A. C. Wilson, K. R. Brown, U. Warring, R. Jördens, J. D. Jost, K. S. McKay, D. P. Pappas, D. Leibfried, and D. J. Wineland, “100-fold reduction of electric-field noise in an ion trap cleaned with *in situ* argon-ion-beam bombardment,” *Phys. Rev. Lett.* **109**, 103001 (2012).
- [12] M. Knoop, I. Marzoli, and G. Morigi (Eds.), *Ion Traps for Tomorrow’s Applications* (IOS, Amsterdam, 2015).
- [13] J. A. Sedlacek, E. Kim, S. T. Rittenhouse, P. F. Weck, H. R. Sadeghpour, and J. P. Shaffer, “Electric field cancellation on quartz by Rb adsorbate-induced negative electron affinity,” *Phys. Rev. Lett.* **116**, 133201 (2016).
- [14] F. Schmidt-Kaler, T. Feldker, D. Kolbe, J. Walz, M. Müller, P. Zoller, W. Li, and I. Lesanovsky, “Rydberg excitation of trapped cold ions: A detailed case study,” *New J. Phys.* **13**, 075014 (2011).
- [15] M. S. Safronova and U. I. Safronova, “Blackbody radiation shift, multipole polarizabilities, oscillator strengths, lifetimes, hyperfine constants, and excitation energies in Ca^+ ,” *Phys. Rev. A* **83**, 012503 (2011).
- [16] M. Aymar, C. H. Greene, and E. Luc-Koenig, “Multichannel Rydberg spectroscopy of complex atoms,” *Rev. Mod. Phys.* **68**, 1015–1123 (1996).
- [17] R. J. Cook, D. G. Shankland, and A. L. Wells, “Quantum theory of particle motion in a rapidly oscillating field,” *Phys. Rev. A* **31**, 564–567 (1985).
- [18] M. Pawlak, N. Moiseyev, and H. R. Sadeghpour, “Highly excited Rydberg states of a rubidium atom: Theory versus experiments,” *Phys. Rev. A* **89**, 042506 (2014).
- [19] G. W. F. Drake, *Atomic, Molecular, & Optical Physics Handbook* (AIP, Woodbury, NY, 1996).
- [20] M. J. Seaton, “Quantum defect theory,” *Rep. Prog. Phys.* **46**, 167–257 (1983).
- [21] Z. Lai, S. Zhang, Q. Gou, and Y. Li, “Polarizabilities of Rydberg states of Rb atoms with n up to 140,” *Phys. Rev. A* **98**, 052503 (2018).
- [22] A. Khadjavi, A. Lurio, and W. Happer, “Stark effect in the excited states of Rb, Cs, Cd, and Hg,” *Phys. Rev.* **167**, 128–135 (1968).
- [23] A. A. Kamenski and V. D. Ovsiannikov, “Formal approach to deriving analytically asymptotic formulas for static polarizabilities of atoms and ions in Rydberg states,” *J. Phys. B: At., Mol. Opt. Phys.* **47**, 095002 (2014).
- [24] J. H. Shirley, “Solution of the Schrödinger equation with a Hamiltonian periodic in time,” *Phys. Rev.* **138**, B979–B987 (1965).
- [25] N. Moiseyev and H. J. Korsch, “Metastable quasienergy positions and widths for time-periodic Hamiltonians by the complex-coordinate method,” *Phys. Rev. A* **41**, 498–501 (1990).
- [26] N. Moiseyev and H. J. Korsch, “Multiphoton dissociation or ionization: Annihilation of discrete quasienergy states in strong electromagnetic fields,” *Phys. Rev. A* **44**, 7797–7803 (1991).
- [27] U. Peskin, O. E. Alon, and N. Moiseyev, “The solution of the time-dependent Schrödinger equation by the (t, t') method: Multiphoton ionization/dissociation probabilities in different gauges of the electromagnetic potentials,” *J. Chem. Phys.* **100**, 7310–7318 (1994).
- [28] U. Peskin and N. Moiseyev, “Time-independent scattering theory for time-periodic Hamiltonians: Formulation and complex-scaling calculations of above-threshold-ionization spectra,” *Phys. Rev. A* **49**, 3712–3728 (1994).
- [29] M. Pawlak, Y. Shagam, A. Klein, E. Narevicius, and N. Moiseyev, “Adiabatic variational theory for cold atom–molecule collisions: Application to a metastable helium atom colliding with *ortho*- and *para*-hydrogen molecules,” *J. Phys. Chem. A* **121**, 2194–2198 (2017).
- [30] M. Pawlak and M. Bylicki, “Stark resonances of the Yukawa potential: Energies and widths, crossings and avoided crossings,” *Phys. Rev. A* **83**, 023419 (2011).
- [31] M. T. Djerad, “Atomic parameters for transitions involving Rydberg states of singly ionized alkaline earths,” *J. Phys. II* **1**, 1–9 (1991).
- [32] C. E. Moore, *Atomic energy levels* (National Bureau of Standards, Washington, DC, 1971).
- [33] The authors in Ref. [4] assigned the excited resonance to the $51F$ state, but subsequent studies [6, 35] revealed that the correct state is $52F$.
- [34] B. M. Smirnov, *Physics of Atoms and Ions* (Springer-Verlag, Berlin, 2003).
- [35] T. Feldker, *Rydberg excitation of trapped ions*, Ph.D. thesis, Johannes Gutenberg-Universität Mainz, 2016.
- [36] F. Schmidt-Kaler (private communication).
- [37] C. Gross, T. Vogt, and W. Li, “Ion imaging via long-range interaction with Rydberg atoms,” *Phys. Rev. Lett.* **124**, 053401 (2020).